SCIENTIFIC REPORTS

OPEN

Optimal fluorescent protein tags for quantifying protein oligomerization in living cells

Received: 14 May 2018
Accepted: 2 July 2018
Published online: 13 July 2018

Valentin Dunsing[1], Madlen Luckner[2], Boris Zühlke[1], Roberto A. Petazzi[1], Andreas Herrmann[2] & Salvatore Chiantia[1]

Fluorescence fluctuation spectroscopy has become a popular toolbox for non-disruptive analysis of molecular interactions in living cells. The quantification of protein oligomerization in the native cellular environment is highly relevant for a detailed understanding of complex biological processes. An important parameter in this context is the molecular brightness, which serves as a direct measure of oligomerization and can be easily extracted from temporal or spatial fluorescence fluctuations. However, fluorescent proteins (FPs) typically used in such studies suffer from complex photophysical transitions and limited maturation, inducing non-fluorescent states. Here, we show how these processes strongly affect molecular brightness measurements. We perform a systematic characterization of non-fluorescent states for commonly used FPs and provide a simple guideline for accurate, unbiased oligomerization measurements in living cells. Further, we focus on novel red FPs and demonstrate that mCherry2, an mCherry variant, possesses superior properties with regards to precise quantification of oligomerization.

A large variety of biological processes relies on transport and interactions of biomolecules in living cells. For a detailed understanding of these events, minimally invasive techniques are needed, allowing the direct quantification of inter-molecular interactions in the native cellular environment. In recent years, fluorescence fluctuation spectroscopy (FFS) approaches have been often used to fulfil this task[1–6]. FFS is based on the statistical analysis of signal fluctuations emitted by fluorescently labelled molecules. While the temporal evolution of such fluctuations provides information about dynamics, the magnitude of the fluctuations contains information about molecule concentration and interactions (i.e. oligomeric state). In order to probe the oligomerization of a protein directly in living cells, the molecular brightness (i.e. the fluorescence signal originating from a single protein complex) can be determined. To this aim, the protein of interest is genetically fused to a fluorescent protein (FP)[4,5,7]. Comparison to a monomeric reference allows the quantification of the number of FP units within a protein complex, i.e. its oligomeric state. For example, a tetrameric protein complex is composed of four protein units, each genetically fused to one FP, and thus the complex carries four FP units in total. The molecular brightness is an average single-molecule quantity, obtained by analysing fluorescence fluctuations of an ensemble of molecules. In a simple scenario, it allows to distinguish whether a sample that emits a certain total fluorescence signal is composed of many dim, or few bright molecules. This analysis can be performed with different experimental methods, e.g. Fluorescence Correlation Spectroscopy (FCS)[1,8], Photon Counting Histogram (PCH)[4,9], Number&Brightness analysis (N&B)[2,7] or subunit counting[10,11]. Differently from other fluorescence based approaches to probe protein oligomerization, such as Fluorescence Resonance Energy Transfer (FRET)[12] or Bimolecular Fluorescence Complementation (BiFC)[13], FFS provides the size of the complex.

Measuring the oligomeric state from the number of fluorescent labels, it is often assumed that all FPs emit a fluorescence signal. However, various *in vitro* studies of FPs revealed complex photophysical properties such as: long-lived dark states of green FPs[14–17], transitions between different brightness states (e.g. YFP[18], mCherry[19]) and flickering[20]. Additionally, limited maturation and folding efficiencies were reported for FPs expressed in cells[21] or as fusions with other proteins[22]. All together, these observations challenge the suitability of FPs for quantitative brightness analysis[5]. In this context, partially contradicting results are reported: studies performing subunit

[1]Institute of Biochemistry and Biology, University of Potsdam, Karl-Liebknecht-Str. 24-25, 14476, Potsdam, Germany. [2]Institute for Biology, IRI Life Sciences, Humboldt-Universität zu Berlin, Invalidenstraße 42, 10115, Berlin, Germany. Valentin Dunsing and Madlen Luckner contributed equally to this work. Correspondence and requests for materials should be addressed to S.C. (email: chiantia@uni-potsdam.de)

counting typically indicate apparent fluorescence probability (p_f) values of 50–80%[10,11,23,24] for GFPs. Very few investigations utilizing FFS approaches report similar values[25,26], while very often it is simply assumed that all FPs are fluorescent. For commonly used red FPs (mainly RFP and mCherry), published results tend to agree, consistently reporting low p_f values (ca. 20–40%)[27,28], with only few exceptions[19].

Notably, many investigations would profit from systematic controls testing the presence of non-fluorescent labels, but so far only few studies take explicitly into account the role of the p_f in the exact quantification of protein-protein interaction[5,11,25,29]. Importantly, oligomerization data are prone to severe misinterpretations if non-fluorescent labels are not taken into consideration, i.e. the molecular brightness of a protein complex may be strongly underestimated. For example, a tetrameric protein complex appears to be a dimer if only one third of all FPs are fluorescent.

To our knowledge, this is the first report systematically comparing non-fluorescent states and associated p_f for various FPs in one-photon excitation. We found significant amounts of non-fluorescent FPs in different cell types and compartments, and we determined the p_f for each FP. With appropriate corrections, we were able to correctly determine the oligomeric state of the homo-trimeric Influenza A virus Hemagglutinin (HA) glycoprotein, for the first time directly in living cells, as a proof of principle.

To investigate multiple interacting molecular species simultaneously, multicolour FFS analysis is often performed. Compared to alternative methods to detect such interactions, e.g. N-way FRET[30], BiFC-FRET[31] or Three-fragment fluorescence complementation (TFFC)[32], it is not constrained to ∼nm distances between the fluorophores and provides an estimate of the true stoichiometry of a protein complex. In multicolour FFS, protein hetero-interactions can be quantified via fluorescence cross-correlation approaches[1,33], even in living multicellular organisms[6,34]. Such methods require well-performing FPs with spectral properties distinguished from the typically used mEGFP. Therefore, current FP development focuses on red and far-red FPs[35]. Nevertheless, the p_f for these proteins, although playing a fundamental role in brightness and cross-correlation analysis, has not been systematically investigated yet. We therefore screened different red FPs for the presence of non-fluorescent states, and found that mCherry2, a not fully characterized mCherry variant, possesses superior properties compared to all other tested red FPs, i.e. mCherry, mCardinal, mRuby3, mScarlet and mScarlet-I. Additionally, by performing Fluorescence Cross-Correlation Spectroscopy (FCCS) measurements of FP hetero-dimers, we show that mCherry2 improves the quantification of the spectral cross-correlation compared to mCherry and propose to use mEGFP and mCherry2 as a novel standard FP pair for hetero-interaction studies.

Results

The brightness of homo-dimers of conventional FPs is lower than double the brightness of monomers. In an ideal case, i.e. if all fluorophores within an oligomer were fluorescent, a homo-dimer would emit twice as many photons as a monomer. We expressed several FPs in the cytoplasm of HEK 293T cells and performed FFS measurements. We found that the brightness values of homo-dimers (normalized to the brightness of the corresponding monomer) for three widely used FPs, namely mEGFP ($\varepsilon_{dimer} = 1.69 \pm 0.05$), mEYFP ($\varepsilon_{dimer} = 1.63 \pm 0.05$) and mCherry ($\varepsilon_{dimer} = 1.41 \pm 0.04$), are generally lower than two, indicating the presence of non-fluorescent proteins. The effect is particularly pronounced for mCherry (Fig. 1a) and does not depend on the specific FFS method used or cellular localization, as shown by comparing the results from N&B, point FCS (pFCS) -in cytoplasm and nucleus- and scanning FCS (sFCS) -for FPs associated to the plasma membrane (PM)- (Fig. 1a,b). Interestingly, we observed a 10% lower brightness for FP monomers within the nucleus compared to the cytoplasmic fraction (Supplementary Figure S1). Furthermore, we measured homo-dimer brightness values of mEGFP and mCherry in different cell lines (HEK 293T, A549, CHO, HeLa) and obtained comparable values in all cell types for the same FP (Supplementary Figure S1).

The maturation time of FPs might influence the fraction of non-fluorescent proteins and this, in turn, may be dependent on the temperature at which experiments are performed[21]. For this reason, we compared the homo-dimer brightness of mEGFP at 23 °C and 37 °C, but observed negligible differences (Supplementary Figure S1).

Taken together, our results demonstrate that the effect of non-fluorescent states on brightness quantification for mEGFP, mEYFP and mCherry is mainly a fluorophore-inherent property and is not strongly influenced by the tested experimental conditions.

The oligomeric state of mEGFP homo-oligomers is correctly determined by using a simple correction scheme for non-fluorescent states. Based on the observed non-fluorescent protein fractions for mEGFP, mEYFP and mCherry, we investigated whether it is possible to nevertheless correctly determine the oligomeric state of higher-order oligomers. To this aim, we expressed mEGFP homo-oligomers of different sizes: 1xmEGFP, 2xmEGFP, 3xmEGFP and 4xmEGFP (i.e. monomers to tetramers). We then performed pFCS measurements in the cytoplasm of living A549 cells (Fig. 2a).

We observed brightness values consistently lower than those expected. For example, the obtained tetramer brightness ($\varepsilon_{tetramer} = 3.01 \pm 0.08$) is very close to the theoretical trimer brightness value (Fig. 2b, white boxes). Hence, we performed a brightness correction based on a simple two-state model[11,36], taking into account the probability that each FP subunit emits a fluorescence signal. The p_f values were determined from the brightness of 2xmEGFP ($\varepsilon_{dimer} = 1.65 \pm 0.06$, $p_f = 0.65$). Thus, we were able to correctly determine the oligomeric state of all mEGFP-homo-oligomers investigated in this study (Fig. 2b, grey boxes). Consistent with the brightness data, pFCS analysis revealed an increase of the diffusion times with increasing homo-oligomer size (Supplementary Figure S2 and related SI).

Furthermore, to extend our investigation to larger protein complexes, we performed N&B measurements on U2OS cells expressing the 12-meric *E. coli* glutamine synthetase (GlnA)[37] (Fig. 2c). We measured an average normalized brightness of $\varepsilon_{GlnA} = 8.8 \pm 0.3$. However, after correction for non-fluorescent mEGFP subunits

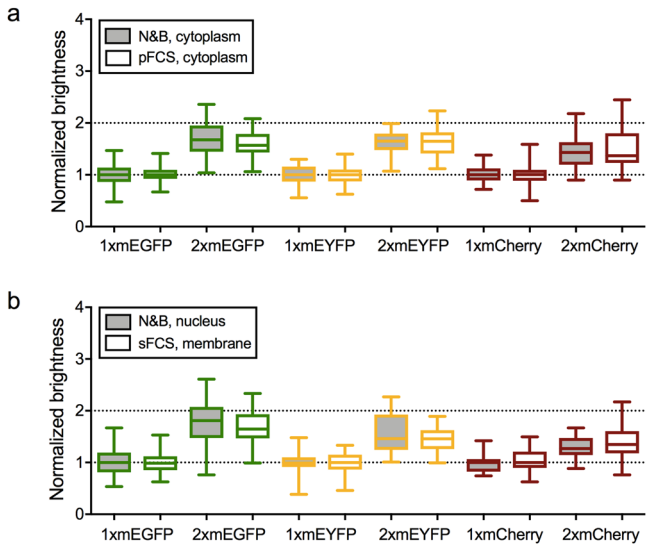

Figure 1. Brightness comparison of different FPs in living HEK 293T cells. (**a**) Box plots of normalized molecular brightness of mEGFP, mEYFP and mCherry monomers and homo-dimers in HEK 293T cells, measured via N&B (grey boxes) or pFCS (white boxes). Monomer and dimer constructs are labeled as "1x" and "2x", respectively. Data were pooled from at least three independent experiments (N&B/pFCS: 1xmEGFP: n = 47/39 cells, 2xmEGFP: n = 48/38 cells, 1xmEYFP: n = 33/37 cells, 2xmEYFP: n = 32/39 cells, 1xmCherry: n = 50/35 cells, 2xmCherry: n = 53/34 cells). (**b**) Box plots of normalized molecular brightness of mEGFP, mEYFP and mCherry monomers and homo-dimers in the nucleus (grey boxes) and PM (white boxes) of HEK 293T cells, measured with N&B (nucleus) and sFCS (PM). For PM measurements, myristoylated-palmitoylated (mp) 1xmEGFP, mp 2xmEGFP, mp 1xmEYFP, mp 2xmEYFP, glycosylphosphatidylinositol-anchored (GPI) 1xmCherry and GPI 2xmCherry constructs were expressed. See Methods section for a description of the investigated FP constructs. Data were pooled from at least three independent experiments (nucleus: 1xmEGFP: n = 47 cells, 2xmEGFP: n = 48 cells, 1xmEYFP: n = 30 cells, 2xmEYFP: n = 32 cells, 1xmCherry: n = 32 cells, 2xmCherry: n = 37 cells; PM: mp 1xmEGFP: n = 55 cells, mp 2xmEGFP: n = 55 cells, mp 1xmEYFP: n = 28 cells, mp 2x mEYFP: n = 28 cells, GPI 1xmCherry: n = 38 cells, GPI 2xmCherry: n = 38 cells).

($\varepsilon_{dimer} = 1.72 \pm 0.05$, $p_f = 0.72$), we obtained an oligomeric state of $\varepsilon_{GlnA} = 11.9 \pm 0.4$, confirming the expected 12-mer structure of the GlnA complex (Fig. 2d).

Overall, these results highlight the importance of performing control experiments with suitable homo-oligomers for brightness-based oligomerization studies and demonstrate that the simple correction for non-fluorescent states presented here produces reliable results.

Influenza A virus hemagglutinin forms homo-trimers in the plasma membrane. We next verified whether the above-mentioned simple two-state brightness correction provides reliable quantitative results in a biologically relevant context. To this aim, we analysed an mEGFP-fused version of the Influenza A virus hemagglutinin (HA-wt-mEGFP), a biochemically well-characterized trimeric transmembrane protein[38,39]. We expressed the fluorescent fusion protein in living HEK 293T cells and performed sFCS measurements (Fig. 3a and Supplementary Figure S3) across the PM. After correction for the non-fluorescent FPs contribution, we obtained an average normalized brightness of $\varepsilon_{HA\text{-}wt\text{-}mEGFP} = 3.17 \pm 0.12$ (Fig. 3b), in line with the expected trimeric structure of HA-wt-mEGFP. We further investigated a hemagglutinin transmembrane domain (HA-TMD-mEGFP) mutant, in which the HA ectodomain is replaced by mEGFP on the extracellular side. This construct was shown to localize as HA-wt-mEGFP in the PM, but in a dimeric form[40]. The observed brightness of HA-TMD-mEGFP was significantly lower than that of HA-wt-mEGFP (Fig. 3b). After correcting for non-fluorescent FPs, we found an average normalized brightness of $\varepsilon_{HA\text{-}TMD\text{-}mEGFP} = 1.82 \pm 0.07$, suggesting the presence of a large dimer fraction.

In summary, these results clearly demonstrate that a simple two-state model for FFS-derived brightness data correction allows precise quantification of the oligomeric state of proteins in living cells.

The mCherry variant "mCherry2" has a superior performance in FFS measurements, compared to other monomeric red fluorescent proteins. In order to extend brightness measurements to the investigation of hetero-interactions, FPs with spectral properties different from those of mEGFP are needed. Typically, red FPs are well suited for this task since spectral overlap with mEGFP is low, reducing the possibility of FRET or cross-talk. However, for the commonly used mCherry, we and others[28] observed a high fraction of non-fluorescent states, i.e. only ca. 40% of the proteins were fluorescent. In order to identify red FPs with higher p_f, we screened the more recently developed FPs mCherry2[41,42], mCardinal[43], mRuby3[44], mScarlet[45] and mScarlet-I[45]. We performed bleaching and N&B measurements of monomers and homo-dimers, expressed in HEK 293T cells. Notably, we observed strong photobleaching for mRuby3, mScarlet and mScarlet-I (Fig. 4a, Table 1) compared to the other three tested FPs. Therefore, N&B measurements on these proteins were conducted

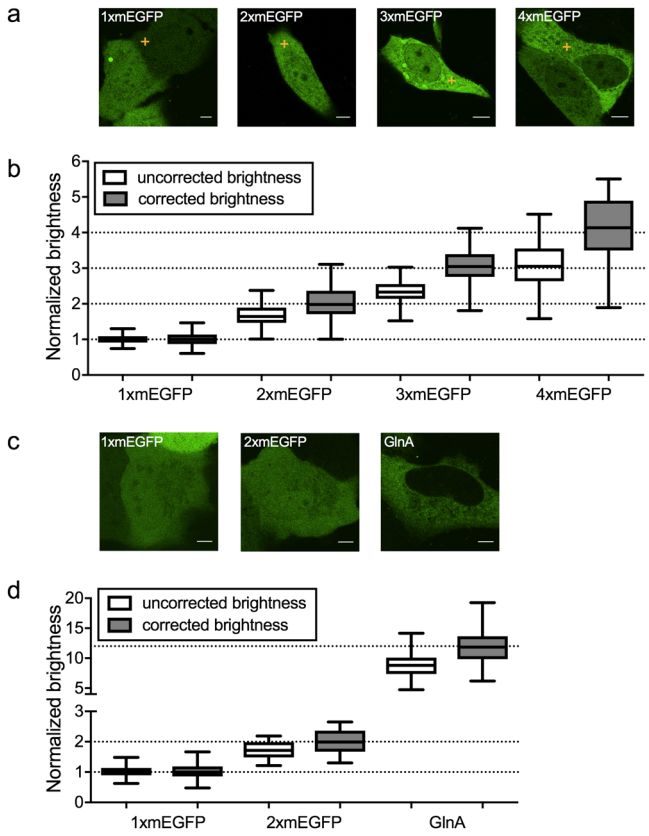

Figure 2. Brightness analysis of mEGFP homo-oligomers. (**a**) Representative intensity images of A549 cells expressing 1xmEGFP, 2xmEGFP, 3xmEGFP and 4xmEGFP, from left to right. Yellow crosses indicate the positions of the pFCS scan point. Scale bars are 5 μm. (**b**) Box plots of normalized molecular brightness obtained from pFCS analysis, pooled from at least three independent experiments (1xmEGFP: n = 52 cells, 2xmEGFP: n = 42 cells, 3xmEGFP: n = 43 cells, 4xmEGFP: n = 59 cells) before correction (white boxes) and after correction (grey boxes). First, a normalization of the uncorrected brightness data was performed using the median brightness value of 1xmEGFP. Second, a correction was performed as described in the Methods section, using a p_f of 0.65, as obtained from measurements of 2xmEGFP. (**c**) Representative intensity images of U2OS cells expressing 1xmEGFP, 2xmEGFP and GlnA-mEGFP (GlnA). Scale bars are 5 μm. (**d**) Box plots of normalized molecular brightness obtained from N&B analysis, pooled from three independent experiments (1xmEGFP: n = 34 cells, 2xmEGFP: n = 35 cells, GlnA: n = 41 cells) before correction (white boxes) and after correction (grey boxes). After normalization using the brightness value of 1xmEGFP, a correction was performed using a p_f of 0.72, as obtained from measurements of 2xmEGFP in U2OS cells.

at lower excitation powers. This reduces their effective brightness, e.g. only 1 kHz for mRuby3, compared to the theoretically three-fold higher brightness when interpolated to the same laser powers used for mCherry, mCherry2 and mCardinal (Fig. 4b). All other FPs exhibit minor difference in the effective brightness ranging from 1.5 kHz (mCherry2) to 2.2 kHz (mCardinal, mScarlet) in our experimental conditions. However, when comparing the normalized homo-dimer brightness, we found strong differences between mCherry2 and the other FPs. We estimated a p_f of 0.71 for mCherry2, which is ~1.8-fold higher than that of mCherry ($p_f = 0.41$) and mScarlet ($p_f = 0.40$), while mCardinal and mRuby3 show very low p_f values of only 0.24 and 0.22, respectively. Notably, mScarlet-I also features a high p_f ($p_f = 0.63$), but still suffers from considerable photobleaching, even at lower excitation powers (Fig. 4c, Table 1).

The superior performance of mCherry2 was confirmed in other cell types, as we consistently observed a reproducible difference from mCherry (Supplementary Figure S4). Moreover, we compared the homo-dimer brightness of mCherry2 at 23 °C and 37 °C and, similarly to mEGFP, observed only negligible variations (Supplementary Figure S4).

We therefore conclude that mCherry2 possesses cell type- and temperature-independent, superior properties in the context of FFS measurements, compared to all the other tested red FPs.

Quantification of hetero-interactions via fluorescence cross-correlation spectroscopy is improved by using mCherry2. Cross-correlation techniques (e.g. FCCS[1], ccN&B[2], RICCS[3]) are powerful methods for the investigation of protein hetero-interactions. These approaches are based on the analysis of simultaneous fluorescence fluctuations emitted by co-diffusing, spectrally distinct labeled molecules. In protein-protein interaction studies, fusion proteins with mEGFP and mCherry or RFP are typically used for this purpose[1,2,6,46].

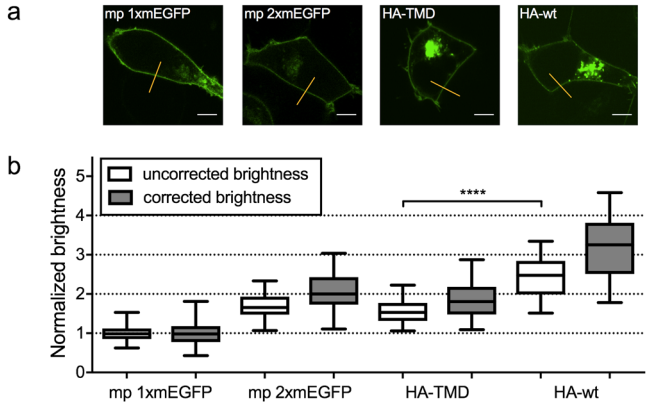

Figure 3. Oligomerization of Influenza A virus hemagglutinin measured with sFCS. (**a**) Representative intensity images of HEK 293T cells expressing mp 1xmEGFP, mp 2xmEGFP, HA-TMD-mEGFP (HA-TMD) and HA-wt-mEGFP (HA-wt), from left to right. Yellow lines indicate sFCS scan lines. Scale bars are 5 μm. (**b**) Box plots of normalized molecular brightness obtained from sFCS analysis, pooled from at least three independent experiments (mp 1xmEGFP: n = 55 cells, mp 2xmEGFP: n = 54 cells, HA-TMD: n = 37 cells, HA-wt: n = 36 cells) before correction (white boxes) and after correction (grey boxes) with $p_f = 0.65$ obtained from mp 2xmEGFP measurements. ****Indicates significance with $p < 0.0001$, obtained by using a two-tailed t-test with Welch's correction.

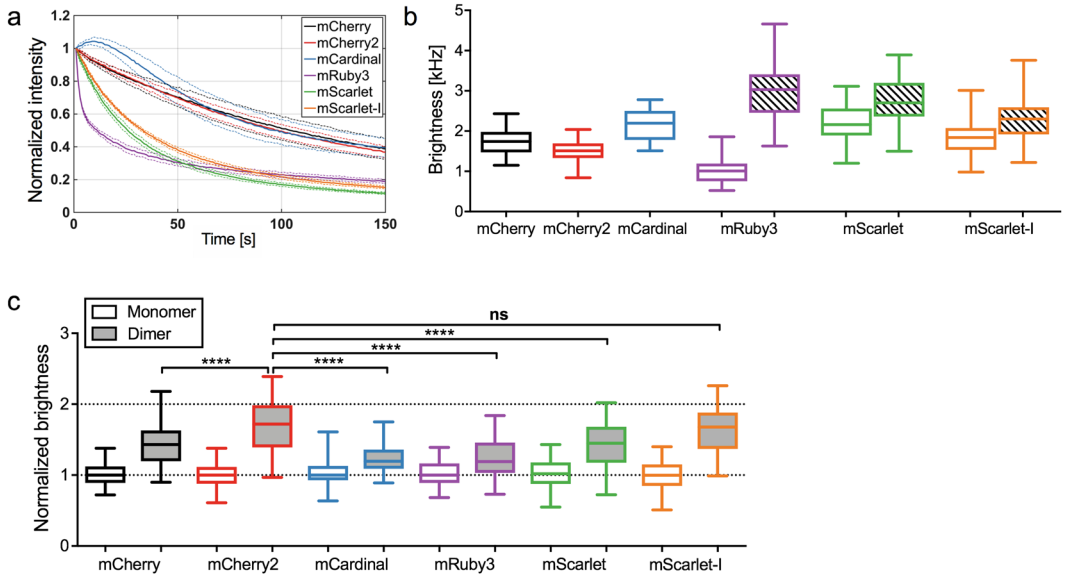

Figure 4. Comparison of different monomeric red FPs in bleaching and N&B measurements. (**a**) Bleaching curves of different red FPs (mCherry, mCherry2, mCardinal, mRuby3, mScarlet and mScarlet-I), expressed in HEK 293T cells, obtained in three independent N&B measurements of 18 cells each, with 19.6 μW laser power (four-fold compared to standard N&B settings). Solid lines show average curves, dashed lines mean ± SD. (**b**) Box plots of molecular brightness of different red FP monomers expressed in HEK 293T cells, measured with N&B at 4.9 μW (mCherry, mCherry2, mCardinal), 3.9 μW (mScarlet, mScarlet-I) or 1.6 μW (mRuby3) laser power in three independent experiments (mCherry: n = 51 cells, mCherry2: n = 49 cells, mCardinal: n = 32 cells, mRuby3: n = 33 cells, mScarlet: n = 36 cells, mScarlet-I: n = 34 cells) (white boxes). The different excitation powers were required to avoid strong bleaching for the less photostable FPs (e.g. mRuby3). The shaded boxes for mRuby3, mScarlet and mScarlet-I show brightness values interpolated to 4.9 μW laser power, assuming a linear increase of the brightness with the excitation power. (**c**) Box plots of normalized molecular brightness of red FP monomers (white boxes) and homo-dimers (grey boxes). Data represent results of three independent experiments (1xmCherry: n = 50 cells, 2xmCherry: n = 53 cells, 1xmCherry2: n = 49 cells, 2xmCherry2: n = 54 cells, 1xmCardinal: n = 42 cells, 2xmCardinal: n = 42 cells, 1xmRuby3: n = 33 cells, 2xmRuby3: n = 31 cells, 1xmScarlet: n = 36 cells, 2xmScarlet: n = 41 cells, 1xmScarlet-I: n = 34 cells, 2xmScarlet-I: n = 39 cells). ****Indicates significance compared to mCherry2 with $p < 0.0001$, ns indicates no significance, obtained by using a one-way ANOVA multiple comparisons test.

FP	$t_{1/2}$* [s]	$t_{1/2,1kHz}$** [s]	$\varepsilon_{N\&B}$ [kHz]	$Bleaching_{N\&B}$ [%]	ε*** [kHz]	p_f
mCherry	104 ± 23	708 ± 156	1.7	6.2	1.7	0.41
mCherry2	99 ± 13	596 ± 80	1.5	4.3	1.5	0.71
mCardinal	97 ± 25	852 ± 220	2.2	−3.5	2.2	0.24
mRuby3	12 ± 1˜	148 ± 12	1.1	37.5	3.1	0.21
mScarlet	26 ± 2˜	280 ± 20	2.2	31.7	2.7	0.40
mScarlet-I	34 ± 1˜	328 ± 12	1.9	29.0	2.4	0.63

Table 1. Characteristics of all investigated monomeric red FPs. *Bleaching half-time ($t_{1/2}$) measured at four times higher laser power (19.6 µW) than used in N&B measurements. **Bleaching half-time ($t_{1/2,1kHz}$) obtained by normalizing the measured half time ($t_{1/2}$) for each FP to an initial brightness of 1 kHz/molecule in the bleaching experiment, using the determined molecular brightness ε of each FP at 4.9 µW. ***Average molecular brightness in N&B, interpolated to the same laser power (4.9 µW) for all red FPs. ˜Experimental conditions differ from those used in the original studies (e.g. spinning disk microscopy vs. confocal microscopy, measurements in cells vs. measurements of purified proteins).

However, due to the presence of non-fluorescent states, only a fraction of protein hetero-complexes simultaneously emits fluorescence in both channels (i.e. many complexes will contain fluorescent green proteins and non-fluorescent red proteins). This factor has to be taken into account when calculating e.g. dissociation constants from cross-correlation data[28]. Given the superior p_f of mCherry2 compared to other red FPs, we hypothesized that mCherry2 would improve the quantification of cross-correlation data, since more complete fluorescent protein complexes should be present. To test this hypothesis, we performed point FCCS (pFCCS) experiments with mCherry-mEGFP and mCherry2-mEGFP hetero-dimers in the cytoplasm of living A549 cells. As presumed, we observed a higher auto-correlation function (ACF) amplitude G in the red than in the green channel ($G_g/G_r = 0.65 \pm 0.03$, Fig. 5a,c) for mCherry-mEGFP, indicating that the apparent concentration of mCherry is ca. 1.5-fold lower than that of mEGFP (i.e. in a significant fraction of hetero-dimers, only mEGFP is fluorescent). This is in agreement with the expected relative amount of hetero-dimers containing fluorescent mEGFP and/or mCherry, based on the above-mentioned p_f values. Furthermore, we expect only ~27% of hetero-dimers to carry both fluorescent mEGFP and mCherry (SI related to Supplementary Figure S5).

For mCherry2-mEGFP in contrast, the amplitudes of the ACFs in the red and green channel were comparable ($G_g/G_r = 0.97 \pm 0.05$, Fig. 5b,c), indicating, as expected, similar apparent concentrations of mCherry2 and mEGFP (SI related to Supplementary Figure S5). Also, the relative amount of hetero-dimers carrying fluorescent mEGFP and mCherry2 is estimated to be ~42%, i.e. 1.5-fold more fully-fluorescent complexes than for mCherry-mEGFP. On the other hand, the expected cross-correlation values for mCherry- and mCherry2-mEGFP should be similar, which is confirmed by our data (Supplementary Figure S5). Nevertheless, the 1.5-fold higher relative fraction of fully-fluorescent hetero-dimers with mCherry2 should improve the quality of cross-correlation data. We therefore compared the signal-to-noise ratio (SNR) of the measured cross-correlation functions (CCFs) for mCherry- and mCherry2-mEGFP, and observed a ~40% higher SNR of mCherry2-mEGFP CCFs ($SNR_{mCh\text{-}mEGFP} = 1.39 \pm 0.10$, $SNR_{mCh2\text{-}mEGFP} = 1.93 \pm 0.10$; Fig. 5d).

These results demonstrate that using mCherry2 instead of mCherry in cross-correlation experiments leads to a more accurate quantification of the spectral cross-correlation, i.e. of the degree of binding in hetero-interactions or the mobility of hetero-complexes.

Discussion

In the last decade, FFS-based techniques have become widely used approaches to measure protein dynamics, interactions and oligomerization directly in living cells and organisms[2,6,34,47–50]. One of the most important quantities in these studies is the molecular brightness, i.e. the photon count rate per molecule, which is used as a measure of oligomerization of fluorescently labelled proteins[4].

In this work, we present a comprehensive analysis of FPs and their suitability for brightness-based oligomerization and cross-correlation-based interaction studies. Differently from previous reports[4,5], we consistently obtained lower than expected values for the normalized brightness of homo-dimers for the most common FPs (i.e. mEGFP, mEYFP and mCherry, Fig. 1a,b). We therefore performed a systematic comparison of frequently used FPs, including also several novel monomeric red FPs (i.e. mCherry2, mRuby3, mCardinal, mScarlet and mScarlet-I), under various conditions. To rule out systematic errors related to the experimental setup or FFS technique used, we performed a combination of pFCS, sFCS and N&B approaches on independent microscopy setups, obtaining reproducible results. Moreover, we excluded potential artefacts deriving from the specific expression system, by comparing different cellular compartments (cytoplasm, nucleus, PM), cell types (HEK 293T, A549, CHO, HeLa) and temperatures (23 °C, 37 °C), as shown in Fig. 1 and Supplementary Figure S1. By performing Fluorescence Lifetime Imaging Microscopy (FLIM) measurements of mEGFP (Supplementary Figure S2), we ruled out the presence of multiple brightness states that might decrease homo-dimer brightness values[19], or energy transfer to non-fluorescent states of mEGFP homo-dimers, in agreement with previous studies[15]. Generally, we cannot rule out the possibility of homo-FRET between the same fluorescent states of homo-dimer subunits. However, as previously discussed, homo-FRET will not affect the brightness of FP homo-dimers[19]. We thus conclude that the observed brightness decrease of FP homo-dimers indicates the presence of a non-fluorescent protein fraction, independent of the experimental conditions. This conclusion is supported by previous reports discussing FP specific photophysical transitions (e.g. blinking, flickering, long-lived dark states)[14–20], maturation times[21]

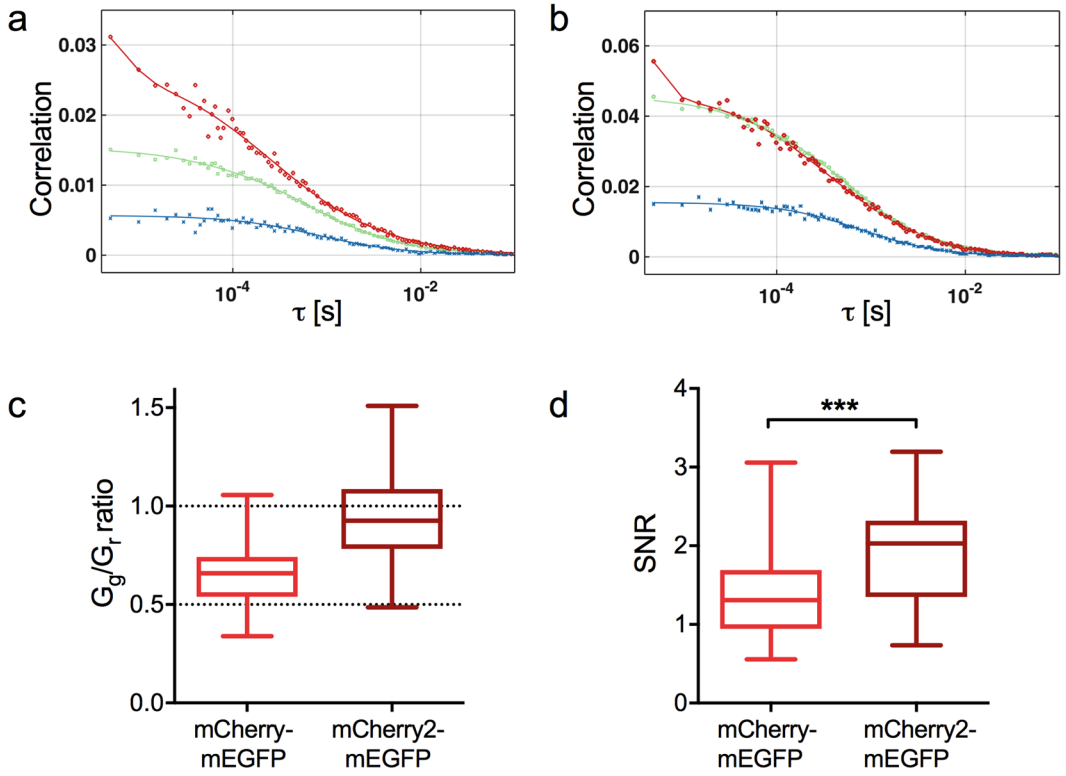

Figure 5. Cross-correlation measurements of mCherry-/mCherry2-mEGFP hetero-dimers. (**a**) and (**b**). Representative correlation functions and fit curves for pFCCS measurements of mCherry-mEGFP (**a**) and mCherry2-mEGFP (**b**) hetero-dimers expressed in A549 cells. Green, ACF in green channel (mEGFP); red, ACF in red channel (mCherry (**a**), mCherry2 (**b**)); blue, CCF calculated for both spectral channels. Fit curves (solid lines) were obtained from fitting a three-dimensional anomalous diffusion model to the data. (**c**) Box plots of amplitude ratios of the green to red ACFs for mCherry-mEGFP (n = 35 cells) and mCherry2-mEGFP (n = 32 cells) pooled from three independent experiments performed in A549 cells. (**d**) Box plots of SNR of the CCFs for mCherry-mEGFP and mCherry2-mEGFP hetero-dimers, calculated from pFCCS measurements in A549 cells, described in (**c**). ***Indicates significance with p = 0.0003, obtained by using a two-tailed t-test with Welch's correction.

and folding efficiencies[22]. For mEGFP, dark state fractions of 20–40% were reported *in vitro*, depending on pH and excitation power[15]. These values agree well with the 25–35% of non-fluorescent mEGFPs that we observed directly in living cells.

We next investigated how the presence of non-fluorescent states exactly affects brightness data of protein complexes of known oligomeric state. This information can then be used to correctly determine the oligomerization state of an unknown protein in general. To this aim, we measured the brightness of mEGFP homo-oligomers as well as two Influenza A virus HA protein variants of different oligomeric states: HA-wt and an HA-TMD mutant. Biochemical studies have shown that the latter proteins assemble as trimers and dimers, respectively[38–40]. We observed a systematic underestimation of the brightness for all samples compared to the expected values (Figs 2, 3) and showed that a simple two-state model, determining the p_f for each FP from the homo-dimer brightness, successfully yields correct estimates of the oligomeric state. Since the assumption of a constant p_f obtained for 2xmEGFP reproduces the correct oligomeric state of higher oligomers, we conclude that folding efficiency and maturation are constant for each single FP subunit within a certain oligomer. In other words, it is sufficient to know the brightness of a FP monomer and homo-dimer, in order to quantify the oligomeric state of larger complexes. It is worth emphasizing that this procedure works well not only for mEGFP homo-oligomers, but also for large self-assembling protein complexes such as the 12-meric *E. Coli* GlnA[37], and transmembrane proteins such as the Influenza A virus HA. An equivalent correction approach was used before in single molecule subunit counting studies, albeit mostly restricted to (m)EGFP[10,11,24]. Our results clearly show that a precise correction of the non-fluorescent FP fraction and knowledge of the p_f for all involved FPs are absolutely necessary for a correct quantification of protein oligomerization in FFS techniques. Ignoring non-fluorescent FPs leads to a strong misinterpretation of the data, e.g. a tetramer being classified as a trimer (Fig. 2). These systematic errors are particularly pronounced for FPs with a low p_f, as found e.g. for mCherry (~40%), a FP often used in the past to determine the stoichiometry of protein complexes[2,51]. Moreover, FPs possessing low p_f severely suffer from low dynamic ranges, since the brightness increase per FP subunit is only marginal (Figs 1, 4), e.g. a mCherry tetramer would be only 2.2 times brighter than a monomer, and could be mistakenly identified as dimer. Nevertheless, contradictory results are reported in this context by studies employing FFS techniques. While very few studies confirm the presence of non-fluorescent mEGFP fractions[25], others report dimer brightness values of 2 (i.e. the absence of a

non-fluorescent FP fraction)[4,5]. However, the latter studies were all performed with two-photon excitation, which may influence the transition to non-fluorescent states[19]. In this context, our data provide the first complete and systematic comparison of p_f for several FPs, in one-photon excitation setups.

In order to measure multiple species simultaneously, red or near-infrared FPs are required due to their spectral separation from mEGFP. Additionally, they are a preferential choice for tissue and animal imaging, due to reduced light absorption and autofluorescence in the red and far-red spectral region[35,52]. Given the suboptimal p_f we determined for mCherry, we screened several recently developed monomeric red FPs[41,43–45]. The p_f is in fact an essential parameter that, until now, has not received appropriate attention in reports of new FPs.

The suitability of FPs for FFS studies depends on three important fluorophore characteristics: (1) a high photostability is required to enable temporal measurements under continuous illumination, (2) a high molecular brightness is needed to obtain a SNR sufficient to detect single-molecule fluctuations, (3) a high p_f is essential for a maximal dynamic range that allows reliable oligomerization measurements. Thus, red FPs which fulfil only one or two of these requirements are not recommended for FFS measurements. Among all red FPs investigated in this study, we found only one fulfilling all three important criteria: mCherry2, a rarely used mCherry variant[41,42] that has not been entirely characterized yet. However, for the remaining red FPs tested here, we found either low photostability albeit high monomer brightness (mRuby3, mScarlet, mScarlet-I; Fig. 4a,b), and/or low to medium p_f of 20–45% (mCardinal, mCherry, mRuby3, mScarlet; Fig. 4c), very similar to previously published values for mRFP[27,28] and mCherry[28]. In contrast, mCherry2 possesses a high p_f of ~70%. Very recent studies of FP maturation times report a faster maturation of mCherry2 and mScarlet-I compared to mCherry/mScarlet[21]. Together with our findings, this indicates that faster FP maturation could be the reason for the observed higher p_f.

Finally, we demonstrate that quantification of hetero-interactions via cross-correlation approaches, so far typically performed with mCherry[1,2,46], can be substantially improved by using mCherry2 instead. In agreement with the reported similar p_f of mEGFP and mCherry2 (Figs 1, 4), we observed that the amount of hetero-dimers containing both fluorescent mEGFP and mCherry2 increased significantly compared to those containing mCherry. For this reason, the CCF signal-to-noise ratio for mCherry2-mEGFP complexes increased by 40% compared to that measured for mCherry-mEGFP hetero-dimers (Fig. 5d). This could be particularly relevant for investigations of weak interactions, in which only a small number of hetero-complexes is present, compared to the vast amount of non-interacting molecules. Additionally, cross-correlation techniques have been recently applied in living multicellular organisms[6,34], which require low illumination to avoid phototoxicity and thus generally suffer from low SNRs. Therefore, we recommend using mCherry2 as the novel standard red FP in brightness and cross-correlation measurements.

In conclusion, this study provides a useful, comprehensive resource for applying FFS techniques to quantify protein oligomerization and interactions. We provide a clear, simple methodology to test and correct for the presence of non-fluorescent states, and argue that such controls should become a prerequisite in brightness-based FFS studies to avoid systematic errors in the quantification of protein oligomerization. Finally, our results suggest that the apparent fluorescence probability is an important fluorophore characteristic that should be considered and reported when developing new FPs and we provide a simple assay to determine this quantity.

Methods

Cell culture. Human embryonic kidney (HEK) cells from the 293T line (purchased from ATCC®, CRL-3216™), human epithelial lung cells A549 (ATCC®, CCL-185™), chinese hamster ovary (CHO) cells from the K1 line (ATCC®, CCL-61™), human epithelial cervix cells HeLa (ATCC®, CCL-2™) and human bone osteosarcoma epithelial cells U2OS (a kind gift from Ana García Sáez, University of Tübingen) were cultured in Dulbecco's modified Eagle medium (DMEM) with the addition of fetal bovine serum (10%) and L-Glutamine (4 mM). Cells were passaged every 3–5 days, no more than 15 times. All solutions, buffers and media used for cell culture were purchased from PAN-Biotech (Aidenbach, Germany).

Fluorescent protein constructs. A detailed description of the cloning procedure of all constructs is available in the Supplementary Information.

All plasmids generated in this work will be made available on Addgene.

Preparation for Microscopy Experiments. For microscopy experiments, 6×10^5 (HEK) or 4×10^5 (A549, CHO, HeLa, U2OS) cells were seeded in 35 mm dishes (CellVis, Mountain View, CA or MatTek Corp., Ashland, MA) with optical glass bottom, 24 h before transfection. HEK 293T cells were preferred for sFCS measurements since they are sufficiently thick and therefore ideal for sFCS based data acquisition perpendicular to the PM. A549 cells are rather flat and characterized by a large cytoplasmic volume that is more suitable for pFCS measurements in the cytoplasm. Cells were transfected 16–24 h prior to the experiment using between 200 ng and 1 μg plasmid per dish with Turbofect (HEK, HeLa, CHO) or Lipofectamin3000 (A549, U2OS) according to the manufacturer's instructions (Thermo Fisher Scientific). Briefly, plasmids were incubated for 20 min with 3 μl Turbofect diluted in 50 μl serum-free medium, or 15 min with 4 μl P3000 per 1 μg plasmid and 2 μl Lipofectamine3000 diluted in 100 μl serum-free medium, and then added dropwise to the cells.

Confocal Microscopy System. Confocal imaging and pF(C)CS measurements were performed on an Olympus FluoView FV-1000 system (Olympus, Tokyo, Japan) using a 60x, 1.2NA water immersion objective. sFCS and N&B measurements were performed on a Zeiss LSM780 system (Carl Zeiss, Oberkochen, Germany) using a 40x, 1.2NA water immersion objective. Samples were excited with a 488 nm Argon laser (mEGFP, mEYFP) and a 561 nm (Zeiss instrument) or 559 nm (Olympus) diode laser (mCherry, mCherry2, mCardinal, mRuby3, mScarlet, mScarlet-I). For measurements with 488 nm excitation, fluorescence was detected between 500 and 600 nm, after passing through a 488 nm dichroic mirror, using SPAD (PicoQuant, Berlin, Germany,

mounted on Olympus instrument) or GaAsP (Zeiss instrument) detectors. For 561 nm or 559 nm excitation, fluorescence emission passed through a 488/561 nm (Zeiss) or 405/488/559/635 nm (Olympus) dichroic mirror and was detected between 570 and 695 nm (Zeiss) or using a 635 nm long-pass filter (Olympus). For pFCCS measurements, fluorophores were excited using 488 nm and 559 nm laser lines. Excitation and detection light were separated using a 405/488/559/635 nm dichroic mirror. Fluorescence was separated on two SPAD detectors using a 570 nm dichroic mirror and detected after passing through a 520/35 nm bandpass filter (mEGFP channel) or a 635 nm long-pass filter (mCherry or mCherry2 channel) to minimize cross-talk.

Fluorescence (Cross-) Correlation Spectroscopy. Point F(C)CS measurements were routinely performed for 90 s and recorded using the SymPhoTime64 software (PicoQuant GmbH, Berlin, Germany). Laser powers were adjusted to keep photobleaching below 20%. Typical values were ~3.3 µW (488 nm) and ~6 µW (559 nm). The size of the confocal pinhole was set to 90 µm. PicoQuant ptu-files containing recorded photon arrival times were converted to intensity time series and subsequently analysed using a custom-written MATLAB Code (The MathWorks, Natick, MA, USA). First, the intensity time series was binned in 5 µs intervals. To correct for signal decrease due to photobleaching, the fluorescence time series was fitted with a two-component exponential function, and a correction was applied[53]. Then, ACFs and, in case of two-colour experiments (g = green channel, r = red channel), CCFs were calculated as follows, using a multiple tau algorithm:

$$G_i(\tau) = \frac{\langle \delta F_i(t)\delta F_i(t+\tau)\rangle}{\langle F_i(t)^2\rangle},$$

$$G_{cross}(\tau) = \frac{\left\langle \delta F_g(t)\delta F_r(t+\tau)\right\rangle}{\left\langle F_g(t)\right\rangle\left\langle F_r(t)\right\rangle},$$

where $\delta F_i = F_i(t) - \langle F_i(t)\rangle$ and $i = g,r$.

To avoid artefacts caused by long-term instabilities or single bright events, CFs were calculated segment-wise (10 segments) and then averaged. Segments showing clear distortions were manually removed from the analysis.

A model for anomalous three-dimensional diffusion and a Gaussian confocal volume geometry was fitted to the ACFs[54]:

$$G(\tau) = \frac{1}{N}\left(1 + \frac{T}{1-T}e^{-\frac{\tau}{\tau_b}}\right)\left(1 + \left(\frac{\tau}{\tau_d}\right)^{\alpha}\right)^{-1}\left(1 + \frac{1}{S^2}\left(\frac{\tau}{\tau_d}\right)^{\alpha}\right)^{-1/2},$$

where the exponential term accounts for photophysical transitions of a fraction T of fluorescent proteins. The parameter τ_b was constrained to values lower than 50 µs for mEGFP[14] or mEYFP[18] and 200 µs for mCherry/mCherry2[20]. The anomaly parameter α was introduced to account for anomalous subdiffusion of proteins in the cytoplasm[54] and constrained to values between 0.5 and 1. The particle number N and diffusion time τ_d were obtained from the fit. To calibrate the focal volume, pFCS measurements with Alexa Fluor® 488 or Rhodamine B dissolved in water at 50 nM were performed at the same laser power. The structure parameter S was fixed to the value determined in the calibration measurement (typically around 4 to 8). The molecular brightness was calculated by dividing the mean count rate by the particle number determined from the fit.

For two-colour measurements, all ACFs were used to fit the diffusion model described above. Relative cross-correlation values were calculated from the amplitudes of ACFs and CCFs:

$$max\left\{\frac{G_{cross}(0)}{G_g(0)}, \frac{G_{cross}(0)}{G_r(0)}\right\},$$

where $G_{cross}(0)$ is the amplitude of the CCF and $G_i(0)$ is the amplitude of the ACF in the i-th channel. The SNR of the CCFs was calculated by summing the cross-correlation values divided by their variance over all points of the CCF. The variance of each point of the CCF was calculated by the multiple tau algorithm[55].

Scanning Fluorescence Correlation Spectroscopy. For sFCS measurements, a line scan of 128 × 1 pixels (pixel size 160 nm) was performed perpendicular to the membrane with 472.73 µs scan time. Typically, 250,000–500,000 lines were acquired (total scan time 2 to 4 min) in photon counting mode. Laser powers were adjusted to keep photobleaching below 20%. Typical values were ~1.8 µW (488 nm) and ~6 µW (561 nm). Scanning data were exported as TIFF files, imported and analysed in MATLAB (The MathWorks, Natick, MA) using custom-written code. sFCS analysis follows the procedure described previously[50,56]. Briefly, all lines were aligned as kymographs and divided in blocks of 1000 lines. In each block, lines were summed up column-wise and the x position with maximum fluorescence was determined. This position defines the membrane position in each block and is used to align all lines to a common origin. Then, all aligned line scans were averaged over time and fitted with a Gaussian function. The pixels corresponding to the membrane were defined as pixels which are within $\pm 2.5\sigma$ of the peak. In each line, these pixels were integrated, providing the membrane fluorescence time series F(t). When needed, a background correction was applied by subtracting the average pixel fluorescence value on the inner side of the membrane multiplied by 2.5σ (in pixel units) from the membrane fluorescence, in blocks of 1000 lines[46]. In order to correct for depletion due to photobleaching, the fluorescence time series was fitted with a two-component exponential function and a correction was applied[53]. Finally, the ACF was calculated as described above.

A model for two-dimensional diffusion in the membrane and a Gaussian focal volume geometry[56] was fitted to the ACF:

$$G(\tau) = \frac{1}{N}\left(1 + \frac{\tau}{\tau_d}\right)^{-1/2}\left(1 + \frac{\tau}{\tau_d S^2}\right)^{-1/2}$$

The focal volume calibration was performed as described for pF(C)CS. Diffusion coefficients (D) were calculated using the calibrated waist of the focal volume, $D = {\omega_0}^2/4\tau_d$. The molecular brightness was calculated by dividing the mean count rate by the particle number determined from the fit: $B = \frac{\langle F(t)\rangle}{N}$.

Number and Brightness Analysis. N&B experiments were performed as previously described[57], with a modified acquisition mode. Briefly, 200 images of 128 × 64–128 pixels were acquired per measurement, using a 300 nm pixel size and 25 µs pixel dwell time. Laser powers were maintained low enough to keep bleaching below 10% of the initial fluorescence signal (typically ~0.7 µW for 488 nm and ~4.9 µW for 561 nm) except for mRuby3 and mScarlet/ mScarlet-I. CZI image output files were imported in MATLAB using the Bioformats package[58] and analysed using a custom-written script. Before further analysis, pixels corresponding to cell cytoplasm or nucleus were selected manually as region of interest. Brightness values were calculated as described[7], applying a boxcar algorithm to filter extraneous long-lived fluctuations[59,60]. Pixels with count rates above 2 MHz were excluded from the analysis to avoid pile-up effects. To further calibrate the detector response, we measured the brightness on a reflective metal surface and dried dye solutions for all laser lines. The thus obtained brightness-versus-intensity plots (which should be constant and equal to 0 for all intensity values[7]) were used to correct the actual experimental data.

Fluorescence Lifetime Imaging Microscopy. FLIM measurements were performed on an Olympus FluoView FV-1000 system (Olympus, Tokyo, Japan) equipped with a time-resolved LSM upgrade (PicoQuant GmbH, Berlin, Germany) using a 60X, 1.2NA water immersion objective. Images of 512 × 512 pixels per frame were acquired after excitation with a pulsed-laser diode at 488 nm. Fluorescence was detected using a SPAD detector and a 520/35 nm bandpass filter. In each measurement, a minimum of 10^5 photons were recorded by accumulation of 60 frames over a time period of 90 s. Regions of interest in the cytoplasm of cells were analysed using SymPhoTime64 software (PicoQuant GmbH, Berlin, Germany) taking into account the instrument response function determined by measuring a saturated Erythrosine B solution according to manufacturer's instructions. Resulting decay curves were fitted using a mono-exponential function.

Brightness calibration and fluorophore maturation. The molecular brightness, i.e. the photon count rate per molecule, serves as a measure for the oligomeric state of protein complexes. This quantity is affected by the presence of non-fluorescent FP fractions, which can result from several processes: (1) Photophysical processes such as long-lived dark states, blinking or flickering between an *on* and *off* state, (2) FP maturation, i.e. FPs that have not maturated yet, (3) Incorrectly folded FPs. To quantify the amount of non-fluorescent FPs, we consider all these processes together in a single parameter, the apparent fluorescence probability (p_f), i.e. the probability of a FP to emit a fluorescence signal. The fluorescence emitted by an oligomer can then be modelled with a binomial distribution, assuming that each fluorophore monomer emits photons with brightness ε and with a probability p_f. The probability of detecting a brightness value iε for an n-mer is thus $p_i = \binom{n}{i} p_f^i (1 - p_f)^{n-i}$. Hence, the ensemble-averaged brightness detected from a number of N n-mers is:

$$\begin{aligned}
\varepsilon_n &= \frac{\sum_{i=1}^{n}(i\varepsilon)^2 N_i}{\sum_{i=1}^{n} i\varepsilon N_i} \\
&= \frac{\sum_{i=1}^{n}(i\varepsilon)^2 N\binom{n}{i} {p_f}^i (1 - p_f)^{n-i}}{\sum_{i=1}^{n} i\varepsilon N\binom{n}{i} {p_f}^i (1 - p_f)^{n-i}} \\
&= \varepsilon\frac{np_f\left(1 - p_f\right) + n^2 {p_f}^2}{np_f} \\
&= \varepsilon + \varepsilon(n-1)p_f
\end{aligned}$$

In the analysis, we normalized all brightness values to the median brightness of the corresponding monomer sample measured under the same conditions: $\varepsilon_{n,norm} = \frac{\varepsilon_n}{\varepsilon} = 1 + (n-1)p_f$. We used the median of the normalized homo-dimer brightness to determine the probability p_f for each construct, $p_f = \varepsilon_{2,norm} - 1$. We can now invert the equation for the n-mer brightness to calculate the true oligomeric state, i.e. the brightness if all subunits were constantly fluorescent, from the measured brightness ε_n: $n = 1 + \frac{\varepsilon_{n,norm} - 1}{p_f}$.

We applied this transformation to every brightness data point and obtained the "corrected" brightness. Notably, this transformation holds true also for fluorophores which have two brightness states rather than an *on* and *off* state[19].

Statistical analysis. All data are displayed as box plots indicating the median values and whiskers ranging from minimum to maximum values. Quantities in the main text are given as mean ± SEM. Sample sizes and

p-values are given in figure captions. Statistical significance was tested using GraphPad Prism 7.0 (GraphPad Software). The one-way ANOVA analysis for comparison of red FPs (Fig. 4b) gave $F(11, 492) = 46.58$ and was followed by the Bonferroni's multiple comparisons test. Brightness differences between HA-wt and HA-TMD (Fig. 3b) as well as SNR of hetero-dimer complexes in FCCS analysis (Fig. 5d) were analysed using a two-tailed t-test with Welch's correction giving Welch-corrected $t = 9.41$, $df = 60.57$ and Welch-corrected $t = 3.84$, $df = 67$, respectively.

Code availability. MATLAB custom-written code is available upon request from the corresponding author.

Data availability. The datasets analysed during the current study are available from the corresponding author on reasonable request.

References

1. Bacia, K., Kim, S. A. & Schwille, P. Fluorescence cross-correlation spectroscopy in living cells. *Nat. Methods* **3**, 83–89 (2006).
2. Digman, M. A., Wiseman, P. W., Choi, C., Horwitz, A. R. & Gratton, E. Stoichiometry of molecular complexes at adhesions in living cells. *Proc. Natl. Acad. Sci. USA* **106**, 2170–2175 (2009).
3. Digman, M. A., Wiseman, P. W., Horwitz, A. R. & Gratton, E. Detecting protein complexes in living cells from laser scanning confocal image sequences by the cross correlation raster image spectroscopy method. *Biophys. J.* **96**, 707–16 (2009).
4. Chen, Y., Wei, L.-N. & Müller, J. D. Probing protein oligomerization in living cells with fluorescence fluctuation spectroscopy. *Proc. Natl. Acad. Sci. USA* **100**, 15492–7 (2003).
5. Chen, Y., Johnson, J., Macdonald, P., Wu, B. & Mueller, J. D. Observing Protein Interactions and Their Stoichiometry in Living Cells by Brightness Analysis of Fluorescence Fluctuation Experiments. in. *Methods in enzymology* **472**, 345–363 (2010).
6. Ries, J., Yu, S. R., Burkhardt, M., Brand, M. & Schwille, P. Modular scanning FCS quantifies receptor-ligand interactions in living multicellular organisms. *Nat. Methods* **6**, (2009).
7. Digman, M. A., Dalal, R., Horwitz, A. F. & Gratton, E. Mapping the number of molecules and brightness in the laser scanning microscope. *Biophys. J.* **94**, 2320–2332 (2008).
8. Elson, E. L. & Magde, D. Fluorescence correlation spectroscopy. I. Conceptual basis and theory. *Biopolymers* **13**, 1–27 (1974).
9. Chen, Y., Müller, J. D., So, P. T. & Gratton, E. The photon counting histogram in fluorescence fluctuation spectroscopy. *Biophys. J.* **77**, 553–67 (1999).
10. Arant, R. J. & Ulbrich, M. H. Deciphering the Subunit Composition of Multimeric Proteins by Counting Photobleaching Steps. *ChemPhysChem* **15**, 600–605 (2014).
11. Ulbrich, M. H. & Isacoff, E. Y. Subunit counting in membrane-bound proteins. *Nat. Methods* **4**, 319–321 (2007).
12. Kenworthy, A. K. Imaging Protein-Protein Interactions Using Fluorescence Resonance Energy Transfer Microscopy. *Methods* **24**, 289–296 (2001).
13. Kerppola, T. K. Bimolecular fluorescence complementation (BiFC) analysis as a probe of protein interactions in living cells. *Annu. Rev. Biophys.* **37**, 465–87 (2008).
14. Haupts, U., Maiti, S., Schwille, P. & Webb, W. W. Dynamics of fluorescence fluctuations in green fluorescent protein observed by fluorescence correlation spectroscopy. *Proc. Natl. Acad. Sci. USA* **95**, 13573–8 (1998).
15. Vámosi, G. *et al*. EGFP oligomers as natural fluorescence and hydrodynamic standards. *Sci. Rep.* **6**, 33022 (2016).
16. Schenk, A., Ivanchenko, S., Röcker, C., Wiedenmann, J. & Nienhaus, G. U. Photodynamics of red fluorescent proteins studied by fluorescence correlation spectroscopy. *Biophys. J.* **86**, 384–94 (2004).
17. Widengren, J., Mets, Ü. & Rigler, R. Photodynamic properties of green fluorescent proteins investigated by fluorescence correlation spectroscopy. *Chem. Phys.* **250**, 171–186 (1999).
18. Schwille, P., Kummer, S., Heikal, A. A., Moerner, W. E. & Webb, W. W. Fluorescence correlation spectroscopy reveals fast optical excitation-driven intramolecular dynamics of yellow fluorescent proteins. *Proc. Natl. Acad. Sci. USA* **97**, 151–6 (2000).
19. Wu, B., Chen, Y. & Müller, J. D. Fluorescence Fluctuation Spectroscopy of mCherry in Living Cells. *Biophys. J.* **96**, 2391–2404 (2009).
20. Hendrix, J., Flors, C., Dedecker, P., Hofkens, J. & Engelborghs, Y. Dark states in monomeric red fluorescent proteins studied by fluorescence correlation and single molecule spectroscopy. *Biophys. J.* **94**, 4103–13 (2008).
21. Balleza, E., Kim, J. M. & Cluzel, P. Systematic characterization of maturation time of fluorescent proteins in living cells. *Nat. Methods* **15**, 47–51 (2017).
22. Pédelacq, J.-D., Cabantous, S., Tran, T., Terwilliger, T. C. & Waldo, G. S. Engineering and characterization of a superfolder green fluorescent protein. *Nat. Biotechnol.* **24**, 79–88 (2006).
23. McGuire, H., Aurousseau, M. R. P., Bowie, D. & Blunck, R. Automating single subunit counting of membrane proteins in mammalian cells. *J. Biol. Chem.* **287**, 35912–35921 (2012).
24. Liebsch, F. *et al*. Full-length cellular β-secretase has a trimeric subunit stoichiometry, and its sulfur-rich transmembrane interaction site modulates cytosolic copper compartmentalization. *J. Biol. Chem.* **292**, 13258–13270 (2017).
25. Godin, A. G. *et al*. Spatial Intensity Distribution Analysis Reveals Abnormal Oligomerization of Proteins in Single Cells. *Biophys. J.* **109**, 710–721 (2015).
26. Slaughter, B. D., Huff, J. M., Wiegraebe, W., Schwartz, J. W. & Li, R. SAM Domain-Based Protein Oligomerization Observed by Live-Cell Fluorescence Fluctuation Spectroscopy. *PLoS One* **3**, e1931 (2008).
27. Hillesheim, L. N., Chen, Y. & Müller, J. D. Dual-Color Photon Counting Histogram Analysis of mRFP1 and EGFP in Living Cells. *Biophys. J.* **91**, 4273–4284 (2006).
28. Foo, Y. H., Naredi-Rainer, N., Lamb, D. C., Ahmed, S. & Wohland, T. Factors affecting the quantification of biomolecular interactions by fluorescence cross-correlation spectroscopy. *Biophys. J.* **102**, 1174–83 (2012).
29. Fricke, F., Beaudouin, J., Eils, R. & Heilemann, M. One, two or three? Probing the stoichiometry of membrane proteins by single-molecule localization microscopy. *Sci. Rep.* **5**, 14072 (2015).
30. Hoppe, A. D., Scott, B. L., Welliver, T. P., Straight, S. W. & Swanson, J. A. N-Way FRET Microscopy of Multiple Protein-Protein Interactions in Live Cells. *PLoS One* **8**, e64760 (2013).
31. Shyu, Y. J., Suarez, C. D. & Hu, C.-D. Visualization of ternary complexes in living cells by using a BiFC-based FRET assay. *Nat. Protoc.* **3**, 1693–1702 (2008).
32. Chen, M. *et al*. Three-Fragment Fluorescence Complementation Coupled with Photoactivated Localization Microscopy for Nanoscale Imaging of Ternary Complexes. *ACS Nano* **10**, 8482–8490 (2016).
33. Schwille, P., Meyer-Almes, F. J. & Rigler, R. Dual-color fluorescence cross-correlation spectroscopy for multicomponent diffusional analysis in solution. *Biophys. J.* **72**, 1878–1886 (1997).
34. Zhao, Z. W. *et al*. Quantifying transcription factor–DNA binding in single cells *in vivo* with photoactivatable fluorescence correlation spectroscopy. *Nat. Protoc.* **12**, 1458–1471 (2017).
35. Cranfill, P. J. *et al*. Quantitative assessment of fluorescent proteins. *Nat. Methods* **13**, 557–562 (2016).
36. Hur, K.-H. *et al*. Quantitative measurement of brightness from living cells in the presence of photodepletion. *PLoS One* **9**, e97440 (2014).

37. Finan, K., Raulf, A. & Heilemann, M. A Set of Homo-Oligomeric Standards Allows Accurate Protein Counting. *Angew. Chemie Int. Ed.* **54**, 12049–12052 (2015).
38. Wilson, I. A., Skehel, J. J. & Wiley, D. C. Structure of the haemagglutinin membrane glycoprotein of influenza virus at 3 Å resolution. *Nature* **289**, 366–373 (1981).
39. Copeland, C. S., Doms, R. W., Bolzau, E. M., Webster, R. G. & Helenius, A. Assembly of influenza hemagglutinin trimers and its role in intracellular transport. *J. Cell Biol.* **103**, 1179–91 (1986).
40. Scolari, S. *et al*. Lateral distribution of the transmembrane domain of influenza virus hemagglutinin revealed by time-resolved fluorescence imaging. *J. Biol. Chem.* **284**, 15708–16 (2009).
41. Shen, Y., Chen, Y., Wu, J., Shaner, N. C. & Campbell, R. E. Engineering of mCherry variants with long Stokes shift, red-shifted fluorescence, and low cytotoxicity. *PLoS One* **12**, e0171257 (2017).
42. Ai, H., Shaner, N. C., Cheng, Z., Tsien, R. Y. & Campbell, R. E. Exploration of New Chromophore Structures Leads to the Identification of Improved Blue Fluorescent Proteins. *Biochemistry* **46**, 5904–5910 (2007).
43. Chu, J. *et al*. Non-invasive intravital imaging of cellular differentiation with a bright red-excitable fluorescent protein. *Nat. Methods* **11**, 572–578 (2014).
44. Bajar, B. T. *et al*. Improving brightness and photostability of green and red fluorescent proteins for live cell imaging and FRET reporting. *Sci. Rep.* **6**, 20889 (2016).
45. Bindels, D. S. *et al*. mScarlet: a bright monomeric red fluorescent protein for cellular imaging. *Nat. Methods* **14**, 53–56 (2017).
46. Dörlich, R. M. *et al*. Dual-color dual-focus line-scanning FCS for quantitative analysis of receptor-ligand interactions in living specimens. *Sci. Rep.* **5**, 10149 (2015).
47. Nagy, P., Claus, J., Jovin, T. M. & Arndt-Jovin, D. J. Distribution of resting and ligand-bound ErbB1 and ErbB2 receptor tyrosine kinases in living cells using number and brightness analysis. *Proc. Natl. Acad. Sci. USA* **107**, 16524–16529 (2010).
48. Hendrix, J. *et al*. Live-cell observation of cytosolic HIV-1 assembly onset reveals RNA-interacting Gag oligomers. *J. Cell Biol.* **210**, 629–46 (2015).
49. Bobone, S. *et al*. Phosphatidylserine Lateral Organization Influences the Interaction of Influenza Virus Matrix Protein 1 with Lipid Membranes. *J. Virol.* **91**, e00267–17 (2017).
50. Dunsing, V., Mayer, M., Liebsch, F., Multhaup, G. & Chiantia, S. Direct evidence of amyloid precursor-like protein 1 trans interactions in cell-cell adhesion platforms investigated via fluorescence fluctuation spectroscopy. *Mol. Biol. Cell* **28**, 3609–3620 (2017).
51. Choi, C. K., Zareno, J., Digman, M. A., Gratton, E. & Horwitz, A. R. Cross-correlated fluctuation analysis reveals phosphorylation-regulated paxillin-FAK complexes in nascent adhesions. *Biophys. J.* **100**, 583–92 (2011).
52. Shcherbakova, D. M. & Verkhusha, V. V. Near-infrared fluorescent proteins for multicolor *in vivo* imaging. *Nat. Methods* **10**, 751–754 (2013).
53. Ries, J., Chiantia, S. & Schwille, P. Accurate Determination of Membrane Dynamics with Line-Scan FCS. *Biophys. J.* **96**, 1999–2008 (2009).
54. Weiss, M., Elsner, M., Kartberg, F. & Nilsson, T. Anomalous subdiffusion is a measure for cytoplasmic crowding in living cells. *Biophys. J.* **87**, 3518–3524 (2004).
55. Wohland, T., Rigler, R. & Vogel, H. The standard deviation in fluorescence correlation spectroscopy. *Biophys. J.* **80**, 2987–99 (2001).
56. Ries, J. & Schwille, P. Studying Slow Membrane Dynamics with Continuous Wave Scanning Fluorescence Correlation Spectroscopy. *Biophys. J.* **91**, 1915–1924 (2006).
57. Digman, Ma., Dalal, R., Horwitz, A. F. & Gratton, E. Mapping the number of molecules and brightness in the laser scanning microscope. *Biophys. J.* **94**, 2320–2332 (2008).
58. Linkert, M. *et al*. Metadata matters: access to image data in the real world. *J. Cell Biol.* **189**, 777–782 (2010).
59. Hellriegel, C., Caiolfa, V. R., Corti, V., Sidenius, N. & Zamai, M. Number and brightness image analysis reveals ATF-induced dimerization kinetics of uPAR in the cell membrane. *FASEB J.* **25**, 2883–2897 (2011).
60. Mayer, M. C. *et al*. Amyloid precursor-like protein 1 (APLP1) exhibits stronger zinc-dependent neuronal adhesion than amyloid precursor protein and APLP2. *J. Neurochem.* **137**, 266–276 (2016).

Acknowledgements

This work was supported by the Deutsche Forschungsgemeinschaft (DFG) grants (254850309 to S.C. and SFB 740, TP C3 to A.H.).

Author Contributions

V.D., M.L. and S.C. conceived the study. V.D., M.L., B.Z. and R.A.P. performed experiments. V.D., M.L. and B.Z. analysed data. V.D., M.L., A.H. and S.C. wrote the manuscript with critical revisions by B.Z. and R.A.P.

Additional Information

Supplementary information accompanies this paper at https://doi.org/10.1038/s41598-018-28858-0.

Competing Interests: The authors declare no competing interests.

Publisher's note: Springer Nature remains neutral with regard to jurisdictional claims in published maps and institutional affiliations.